

Exploring Scaling Relations and Active Site Specificity of Graphite-Conjugated Catalysts Using Density Functional Theory

Nathan D. Ricke,¹ Kelly Chen,¹ Troy Van Voorhis^{1*}

¹Department of Chemistry, Massachusetts Institute of Technology, Cambridge, Massachusetts 02139, United States

*Corresponding Author. Email: tvan@mit.edu. Phone: 617-253-1488

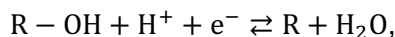
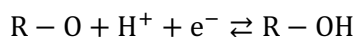
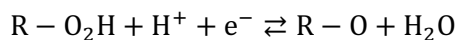
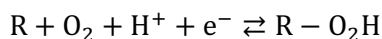
Abstract

Graphite-conjugated catalysts (GCC) are a class of highly synthetically tunable materials with properties of both homogeneous and heterogeneous catalysts. GCCs have proven especially promising for catalyzing the oxygen reduction reaction (ORR). In this study, we applied density functional theory (DFT) to explore how functional group and aromatic scaffold modifications affect catalytic activity of GCCs for ORR. We found that both kinds of modifications can have a significant enough effect on catalytic activity to tune the ORR rate determining step between the strong and weak oxygen binding regimes. Further, we found that DFT predicts certain GCC scaffolds could have an epoxide intermediate during the catalytic cycle instead of the more usually predicted atomic oxygen bound to a single site. We also investigated patterns in the effects of functional group modifications, and under what conditions it is possible to break scaling relations for these catalysts. Our findings provide a deeper understanding of why ORR activity is limited to specific aromatic carbon active sites in GCCs, elucidating general principles for designing ORR catalysts with nitrogen-doped aromatic carbon materials.

1. Introduction

The oxygen reduction reaction (ORR) is the reduction of oxygen to water, which releases energy that can be used to generate electricity.¹ In terms of the efficiency of electricity generation, electrochemical fuel cells containing an appropriate catalyst are more efficient than burning H₂ and O₂ to generate heat to run a turbine. The best catalysts for ORR contain platinum,^{1,2} and while alternative materials have been considered,³⁻⁵ it has proven quite challenging to optimize the efficiency of ORR electrocatalysts.^{6,7}

In terms only of the efficiency of ORR, articulating the effect of this ideal electrocatalyst on the catalytic cycle is easy, but rather difficult to actualize. The ideal electrocatalyst would harvest the same amount of energy per electron transferred in each step of the overall electrochemical reaction $4\text{H}^+ + 4\text{e}^- + \text{O}_2 \rightarrow 2\text{H}_2\text{O}$. The associative reaction mechanism,⁸ the mechanism generally understood to occur for many successful ORR catalysts, proceeds through the steps,



where R is the electrocatalyst.⁷ As four electrons are transferred and the overall free energy of reaction is -4.92 eV, this ideal catalyst would cause each of these step's reaction energy to be -1.23 eV. In terms of the voltage of an electrochemical cell, each step would have a current when the cell is at 1.23 V relative to the reversible hydrogen electrode, and would have zero overpotential because this is the maximum possible voltage at which the reaction could proceed.⁹

Scaling relations between intermediate reaction energies are the primary reason that the ideal ORR electrocatalyst is so elusive.⁶ In general, a scaling relation in a catalytic cycle is the correlation between the intermediate reaction energies of two steps in the cycle over a range of different catalysts.^{7,10} The most well-known of these scaling relations is the relatively linear relationship between the intermediate reaction energies of $\text{R} + \text{O}_2 + \text{H}^+ + \text{e}^- \rightleftharpoons \text{R} - \text{O}_2\text{H}$ and $\text{R} - \text{OH} + \text{H}^+ + \text{e}^- \rightleftharpoons \text{R} + \text{H}_2\text{O}$, which is caused by the fact that active sites that bind one oxygen species strongly, such as O₂H, are likely to strongly bind to other oxygen species, such as OH.⁶ This is especially apparent for these two steps because they each involve forming and breaking bonds between the catalyst and an oxygen species.

Within the framework of understanding provided by scaling relations, ORR catalyst design strategies can be classified as either seeking to modify an existing catalyst to push the new catalyst closer to the optimal oxygen binding strength along the scaling relations, or to favorably break these scaling relations. Although the latter would be necessary to obtain the ideal catalyst

starting from all currently known catalysts, the former method could potentially be productively applied to obtain catalysts with similar activity to state-of-the-art platinum catalysts with less expensive materials. In either case, systematically optimizing a catalyst requires a degree of synthetic tuneability generally only available to homogeneous catalysts, which are not as straightforward to separate from the reaction products and operate continuously in industrial applications.¹¹

One class of catalysts that combines synthetic tuneability with the advantages of heterogeneous catalysts are graphite-conjugated catalysts (GCCs).¹² GCCs are an advantageous model system because they enable the exploration of a large chemical space, which is relatively uncommon for heterogeneous catalysts. The chemical space of GCCs is large because there are many types of catalysts that could be conjugated directly to graphite: the actual synthesis only requires a diamine a molecule to be conjugated, with the only additional requirement being that the molecule cannot have any functional groups that will interfere with the condensation reaction.¹² Broadly, this leads to a chemical space not dissimilar to small molecule drugs, estimated to contain on the order of 10^{60} distinct systems.¹³ GCCs' chemical space is also as of this time relatively unexplored relative to the vast scale of small molecules that could be conjugated.¹² A variety of GCCs have been developed, including both organometallic^{14–17} and organic^{18–20} catalysts designed for distinct reactions, demonstrating the value of exploring the depth of this chemical space further.

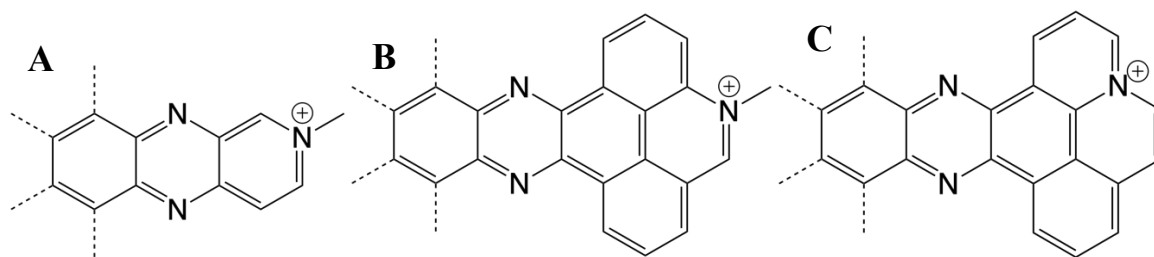


Figure 1: The three exploratory catalysts initially designed in this study to investigate tunability of N^+ -GCC systems.

This study focuses on how differences in GCC structures affect the intermediate reaction energies in ORR, with a particular focus on which kinds of modifications shift the catalyst along or cause deviations from the known scaling relations. We applied density functional theory (DFT)^{21,22} to calculate these reaction energies, as DFT is sufficiently inexpensive to enable the exploration of many structures. In this work we chose to consider functional group modifications of three initial GCC structures, which were each elaborations of a known GCC (**Figure 1**).¹² We chose the composition of these structures specifically to study how differences in the carbon scaffold around the cationic nitrogen affect the active sites. Each of these base structures has similar probable active sites, namely carbon atoms ortho to the cationic nitrogen, but we had no definite knowledge of which sites would be active prior to this study. Previous work by Lodaya et al. provided a thorough statistical analysis of ORR active sites on a variety of GCC structures, showing that cationic nitrogen typically activate secondary carbons that are an odd number of bonds away from

the nitrogen, which provided the initial hint that these catalysts may have non-ortho active sites as well.²³

In this work, we expanded the statistical understanding of GCC design space by systematically exploring functional group derivatives of each of the three base structures. We generated derivatives of each of these structures and analyzed how these functional group modifications affect likely catalytic activity. We found that the structure of the carbon scaffold largely determines the active site location. The location of these active sites correspond to reactive carbons identified by Clar structures,²⁴ which rationalize why only specific carbons near cationic nitrogen bind oxygen in these catalysts. We also explored derivative substitutions of these catalysts, demonstrating that derivatization can be applied to tune intermediate energies, with substitutions at specific locations near the active site having especially strong effect. Derivatives that donate electron density generally increase the binding strength of oxygen intermediates, whereas electron withdrawing groups have the reverse effect, but the effect can be more complex when modifications interact directly with the active site through the aromatic structure. This analysis of the effect of modifying the carbon structure and derivatives of GCCs provides insight on aromatic carbon active sites that can be generalized to nitrogen-doped carbon materials.

2. Computational Methods

Density Functional Theory

We performed all DFT calculations using the ab-initio software package Q-Chem,²⁵ using the meta-hybrid functional TPSSH²⁶ and the basis set 6-31G*.²⁷⁻²⁹ To model solvation, we used the implicit solvation model IEF-PCM with a dielectric constant of 78.4.³⁰ To obtain structures, we used MMFF94³¹ to pre-optimize the geometry followed by DFT. All molecular images were generated using the software packages ChemDraw and VESTA.³² We used the procedure described by Mavros et al.³³ to compute the free energy of each intermediate in the catalytic cycle for the catalysts in this study, designated by A, B, and C in **Figure 1**.

Functional Group Modification

To evaluate the effect of individual functional groups on the energy of each intermediate reaction step in the ORR catalytic cycle, we generated an enumerative library of catalysts with hydrogen replaced by functional groups. The full set of functional groups used to replace hydrogens atoms is shown in **Figure 2**. For catalysts A, B, and C, we generated all possible catalysts with a single functional group substitution, producing to 33 derivatives of catalyst A, 88 derivatives of catalyst B, and 77 derivatives of catalyst C. For catalysts B and C, we additionally generated a number of possible catalysts with two functional group substitutions, producing 126 derivatives of catalyst B and 338 derivatives of catalyst C. We used RDKit's python library to produce these functional group substitutions and generate initial geometries.³⁴ We used DFT to optimize all functionalized catalysts. We subsequently used these DFT optimized geometries as inputs to a python script we wrote to produce initial guesses for the geometry of the catalytic cycle intermediates O₂, O₂H, O, and OH. We then optimized all these intermediates with DFT and computed the free energy of

each reaction step (SI section 1). We also computed the difference between the intermediate reaction energies of the derivatized catalyst and its corresponding underivatized catalyst, which directly measures the effect of each functional group on the catalytic cycle energetics.

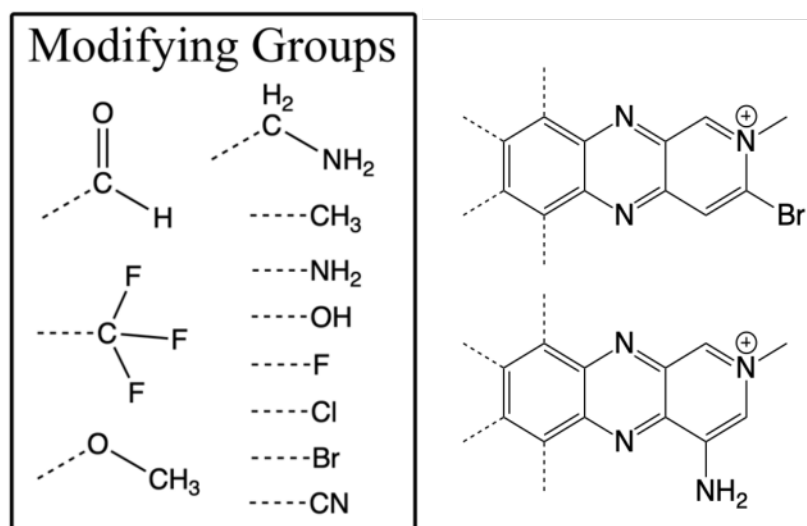


Figure 2: Left: Functional groups used to modify catalysts. Right: Examples of catalyst A modified by functional groups at two different positions. The functional group substitutions were made on all hydrogen atoms not directly connected to active site carbon atoms.

Principal Component Analysis

Principal component analysis (PCA) is a mathematical tool that can be applied to identify which independent variables contribute most strongly to the variance of a dependent variable, and to elucidate relations between independent variables in how they cause this variance. We applied PCA to quantify which functional group substitution locations most strongly affect the intermediate reaction energies of ORR and to determine similarities between functional groups in how they affect these energies. Section 2 of the SI contains a detailed discussion of the mathematics of how we applied PCA within this context.

3. Results and Discussion

Catalyst Active Sites

In order to predict the ORR activity of the catalysts in this study, we initially had to find the location of their active sites. Ricke et al. observed in a previous study that localized spin density of the oxidized species indicated the active site on a GCC very similar to catalyst A in this study,³⁵ so we plotted the spin density on each of the more novel catalysts B and C (**Figure 3**). For catalyst B, the highest spin density is localized on a single carbon atom, whereas for catalyst C there are two carbon atoms that have relatively similar spin densities. We placed O₂ near each sp² carbon atom in the catalytic region of these molecules and found that the only atoms that bound O₂ favorably were the very same carbons indicated by the spin density localization (**Figure 4**).

Lodaya et al. previously found that cationic nitrogen in GCCs can act as ortho-para activators for O_2 binding, which is in line with the active site locations observed in this work.³⁶

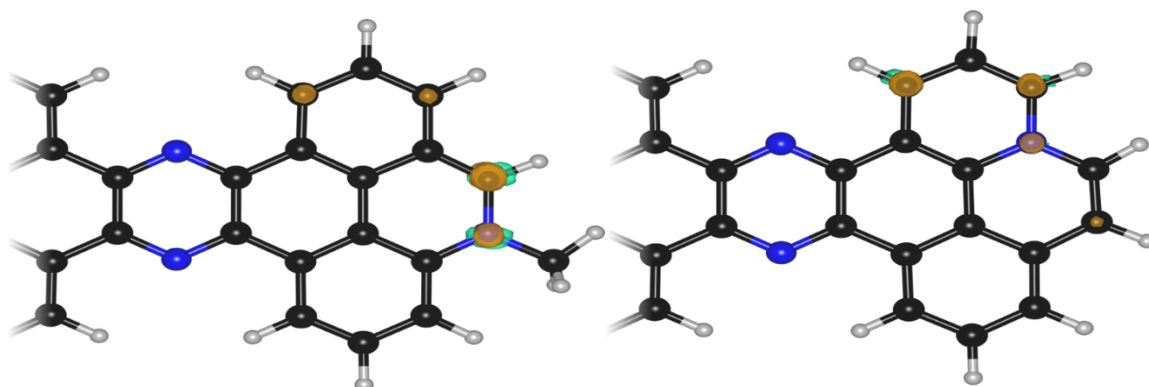


Figure 3: Spin density plots shown for catalysts B (left) and C (right). For catalyst B, the highest spin density is definitively localized on a single carbon, whereas for catalyst C the highest spin density localization is split between two carbon atoms.

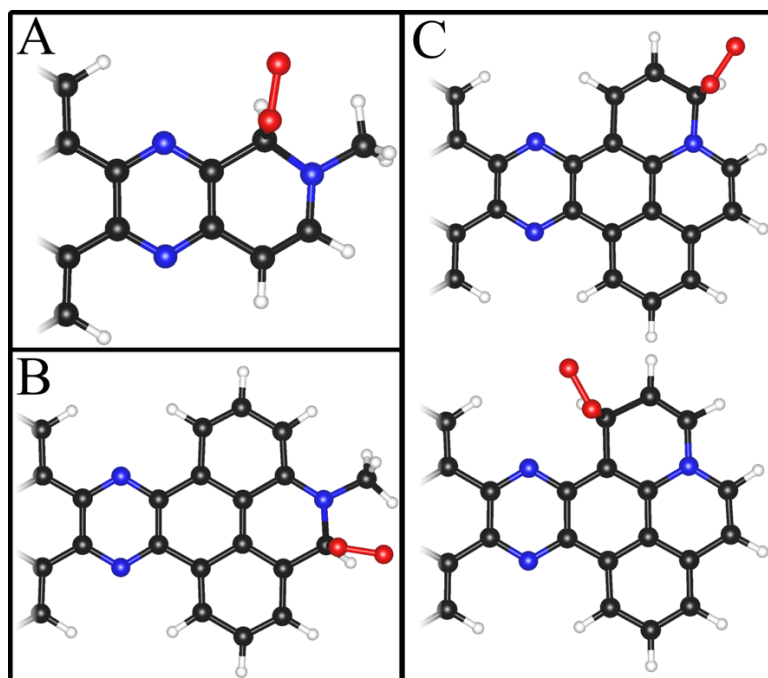


Figure 4: The active sites for each of the three catalysts are shown by where O_2 bound to the catalyst with a favorable binding energy. For catalyst C, two distinct carbon atoms are active for binding O_2 and catalyzing ORR.

Unlike the other ORR intermediates in this study, the O intermediate in catalyst C is unique in that it bonds directly to two carbons to form an epoxide intermediate. We discovered this epoxide intermediate when we placed the O atom at the ortho active site and optimized the geometry of the system, which caused the O atom to spontaneously transition into epoxide intermediate

(Figure 5). We calculated the energy of the epoxide structure relative to the single-site bound O atom at the ortho active site and found the epoxide structure is 0.06 eV lower in energy. Using the freezing string method,^{37,38} we calculated the activation energy for the transition between the two states to be 0.17 eV to transition from the single-site to epoxide structure. This energy difference is small enough that interconversion between both these binding modes would be possible during catalysis. We found that although the para active site can similarly form an epoxide structure by binding to the the same meta carbon as the ortho epoxide, this epoxide structure would not form spontaneously during DFT optimization from the single site O intermediate initial geometry.

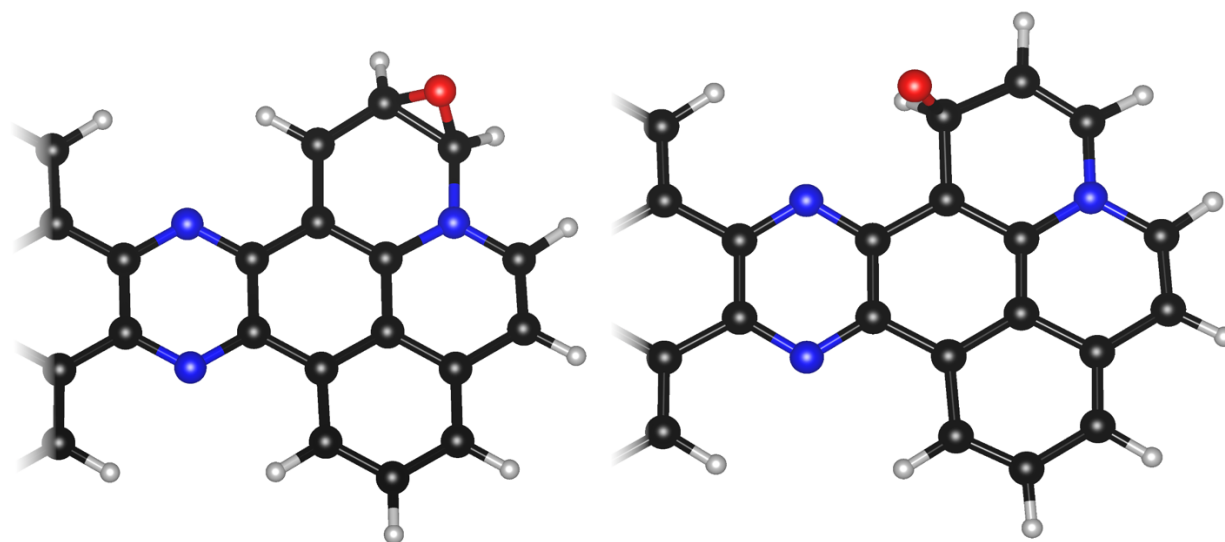


Figure 5: The oxyl moiety binds to catalyst C in two different ways. At the para active site, the oxyl moiety forms a single to that active site, whereas at the ortho position it forms an epoxide, binding across both the ortho and meta positions.

The specificity of where O₂ will bind, as well as whether an epoxide intermediate will form for the R-O intermediate, can be explained by oxygen's tendency to bind to carbons that are not part of rings in Clar structures.^{24,39} The premise behind Clar structures is that not all carbon atoms in polyaromatic systems are equally stable, and unstable carbons can be identified based on the resonance structures of the system. Clar structures predict that the most stable resonance structure is the one with the maximum number of nonadjacent aromatic rings. Further, any aromatic carbon atoms that are not part of rings in the most stable Clar structure will be more reactive. The formalism of Clar structures also introduces an arrow notation that summarizes multiple resonance structures with the same number of total aromatic rings; the carbons in these rings are considered more stable than ones that are not in any ring.

When generating Clar structures for these catalysts with the assumed constraint that their cationic nitrogen atoms cannot be in aromatic rings, we found that the Clar structures identify the active sites in each catalyst. While there are no aromatic rings that can be drawn in the Clar structure

for catalyst A without including nitrogen, the active carbon is the only location where O_2 may bind that breaks aromaticity of only the cationic nitrogen, and thus avoiding the destabilization of other carbons in the catalyst. For catalyst B, the Clar structure identifies three carbons that are not part of rings, but the carbon adjacent to the cationic nitrogen is the only active site because binding O_2 to the other carbons would either leave the adjacent carbon with a radical electron or require reducing the number of rings in the Clar structure (**Figure 6**). For catalyst C there are five carbons outside of aromatic rings in the Clar structure, but the two active sites are once again determined by where O_2 can bind without disrupting the octet of surrounding carbons. Beyond catalytic activity, these Clar structures bear a strong resemblance to the spin density plots of these catalysts (**Figure 3**), and may provide a predictive tool for identifying N^+ -GCC active sites without use of DFT.

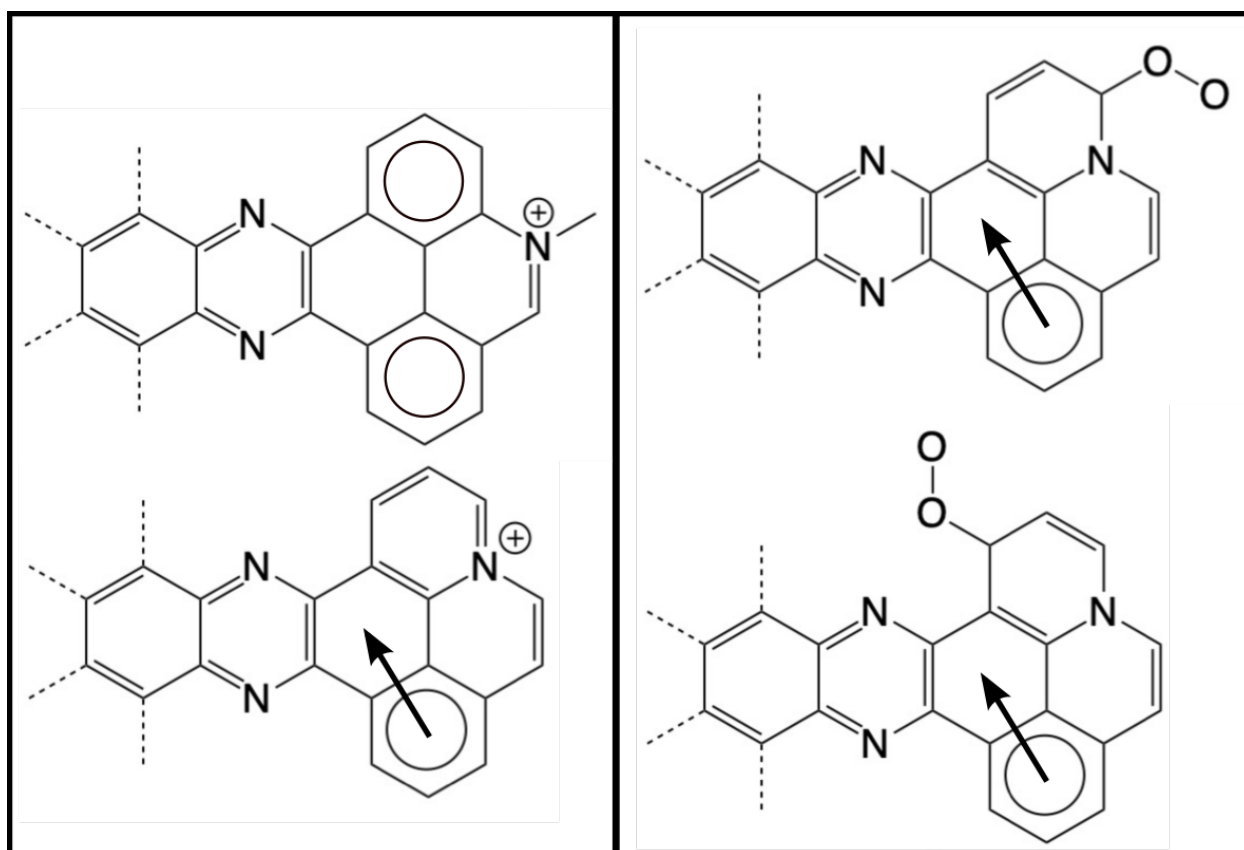


Figure 6: Left: Clar structures for catalysts B and C. Right: Clar structures for catalyst C with O_2 bound to each active site.

Table 1: Free energy of reaction for catalyst A, B, and C for each intermediate in the ORR catalytic cycle. Catalyst C's two active sites are represented as C-1 and C-2.

Catalyst	Free Energy of Reaction (eV)				
	R → R-	R-O ₂ → R-	R-O ₂ H → R-	R-O → R-	R-OH →
A	0.22	-0.67	-1.71	-1.75	-0.79
B	-0.07	-0.89	-1.73	-1.75	-0.55
C-1	0.21	-0.56	-1.75	-1.78	-0.84
C-2	0.07	-0.70	-2.14	-1.45	-0.63

We used the active sites and intermediates to calculate the reaction free energy for each intermediate in the catalytic cycle for catalysts A, B, and C, designating for catalyst C the active site para to the cationic nitrogen as C-1 and the ortho site as C-2 (**Table 1**). The values in **Table 1** are the energy minima for the intermediates, and do not account for the barrier height of the transitions between intermediates. These values indicate that the reactions $R - O_2H \rightarrow R - O$ and $R - O \rightarrow R - OH$ are not thermodynamic barriers, similar to the previously studied GCC.³⁵ Independent of whether the chemical step $R \rightarrow R - O_2$ is grouped with the electrochemical step $R - O_2 \rightarrow R - O_2H$, the electrochemical process of forming $R - O_2H$ is the likely source of the overpotential for catalysts A and C-1, placing them in the weak-binding regime of ORR catalysts. Catalysts B, on the other hand, is likely limited by $R - OH \rightarrow R$, placing it in the strong-binding regime. Catalyst C-2 is quite close to the threshold between these regimes, and its classification would depend on the kinetics of how $R - O_2H$ is formed. One particularly interesting feature of catalyst C is the marked difference between these active sites despite their proximity and chemical similarity; although the scaling relation between the first and last steps are not significantly affected, the epoxide intermediate has a significant effect on the steps involving $R - O$.

Effects of Functional Group Modification

Having observed the notable differences between catalysts A, B, and C in ORR intermediate energies, we considered next the effects of functional group modifications. **Figure 2:** Left: Functional groups used to modify catalysts In order to understand how these catalysts differ in their ORR scaling relations, we generated a pair plot to visualize the correlations between all intermediate reaction steps in the catalytic cycle (**Figure 7**). The subplots along the diagonal of **Figure 7** show the density of catalysts spread across intermediate step reaction energies, whereas the off-diagonal subplots show how correlated the energies of two different reaction steps are for a given catalyst.

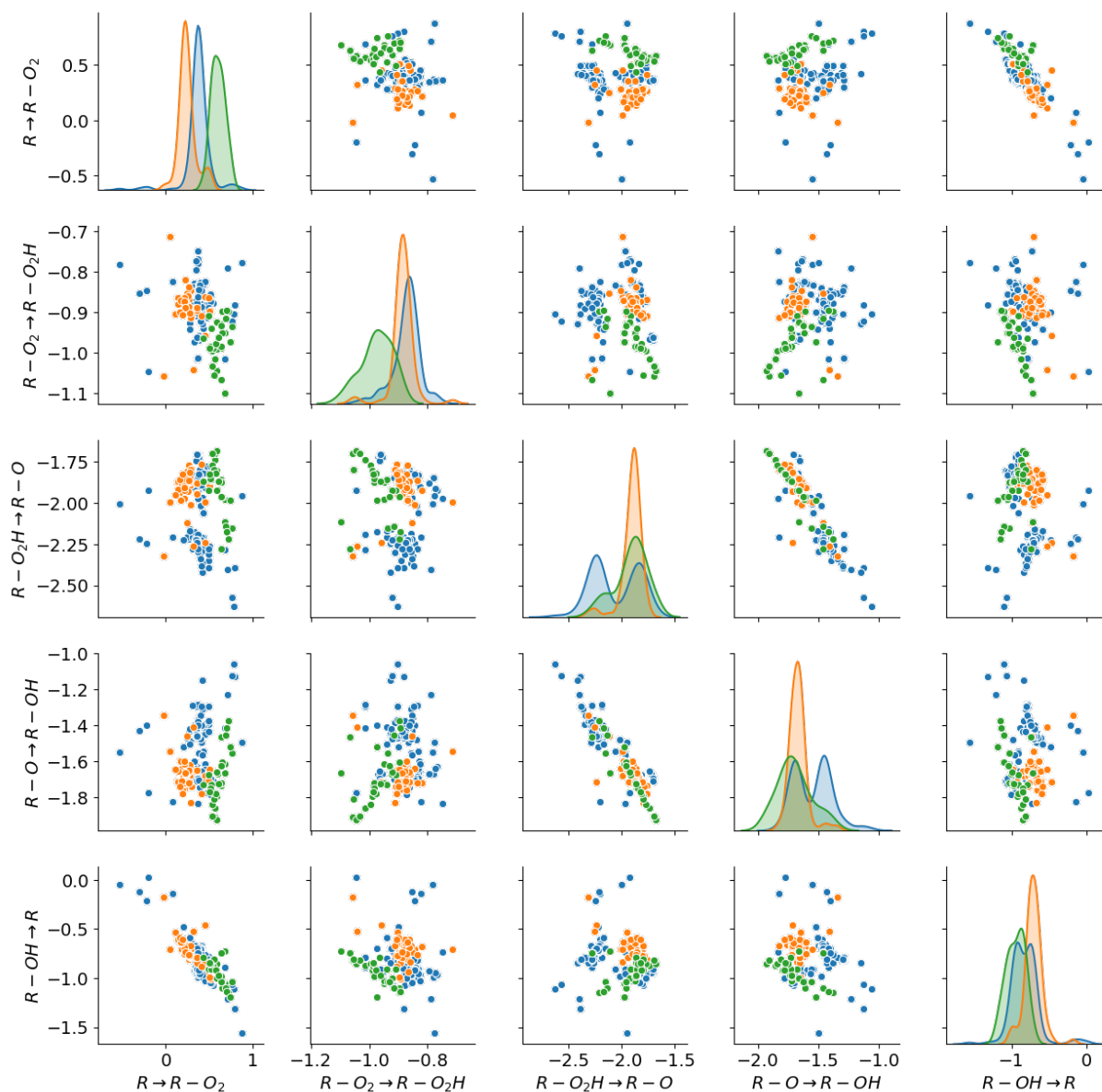


Figure 7: Pair plot of intermediate energy correlations for the ORR catalytic cycle. Along the diagonals are the densities of each intermediate across an energy range. All energies are shifted such that the intermediate energies for catalyst A are centered on 0. The green points are catalyst A, the orange points are catalyst B, the blue points are catalyst C.

This representation of the data is useful for visualizing correlations between all reaction energies in the catalytic cycle. **Figure 7** depicts two scaling relations that hold across all three of the catalysts: the steps $R \rightarrow R - O_2$ vs $R - OH \rightarrow R$ with a correlation coefficient of 0.82, and $R - O_2H \rightarrow R - O$ vs $R - O \rightarrow R - OH$ with a correlation coefficient of 0.92. The former is analogous to the well-known tradeoff between strong and weak oxygen binding catalysts, whereas the latter has received less attention because neither step is typically a thermodynamic barrier in the catalytic cycle. This second O_2 correlation is nonetheless important because it depicts why the

unnecessarily exothermic oxygen-oxygen bond breaking is difficult to optimize: as $R - O_2H \rightarrow R - O$ moves closer to the optimal -1.23 eV, $R - O \rightarrow R - OH$ is already below -1.23 eV. Similar to other known scaling relations, this one must also be broken to obtain the optimal catalyst. Although the epoxide intermediate for catalyst C-1 does not break the scaling relation involving $R - O_2H \rightarrow R - O$ vs $R - O \rightarrow R - OH$, it does create a bimodal distribution visible on the diagonals of **Figure 7** for each of the reactants where the epoxide is present as either the initial or final state.

To draw a direct comparison to other kinds of catalysts, we constructed a volcano plot for catalytic activity (**Figure 8**). This volcano plot is essentially a specific pair plot analogous to **Figure 7** comparing the intermediate reactions $R \rightarrow R - O_2H$ and $R \rightarrow R - OH$. This comparison is especially important because catalytic activity is often limited by one of these two steps; when limited by the former the catalyst is in the weak-bonding regime and for the latter the strong-binding regime. These two intermediate reactions can often be examined to the exclusion of other catalysts because breaking the O-O bond in the step $R - O_2H \rightarrow R - O$ is typically very exothermic, and the reaction $R - O \rightarrow R - OH$ is generally not rate limiting because the $R - O$ intermediate is very often much less stable than the $R - OH$ intermediate. **Figure 8** shows that catalyst A's derivatives generally fall in the weak-bonding regime and catalyst B's fall in the strong-bonding regime, whereas catalyst C's derivatives fall on either side of this tradeoff.

As seen in **Figure 7** and **Figure 8**, both derivatization and the structure of the carbon-nitrogen scaffold around the active site can significantly affect catalytic activity. Although significant, the effect of both factors on the reactions $R \rightarrow R - O_2H$ and $R \rightarrow R - OH$ is strongly correlated. To a small extent, the change in active site between C-1 and C-2 exhibits a small deviation from this scaling relation, along with a handful of derivatives of C-1, for which the effects of derivatization are significantly more pronounced than all the other GCCs.

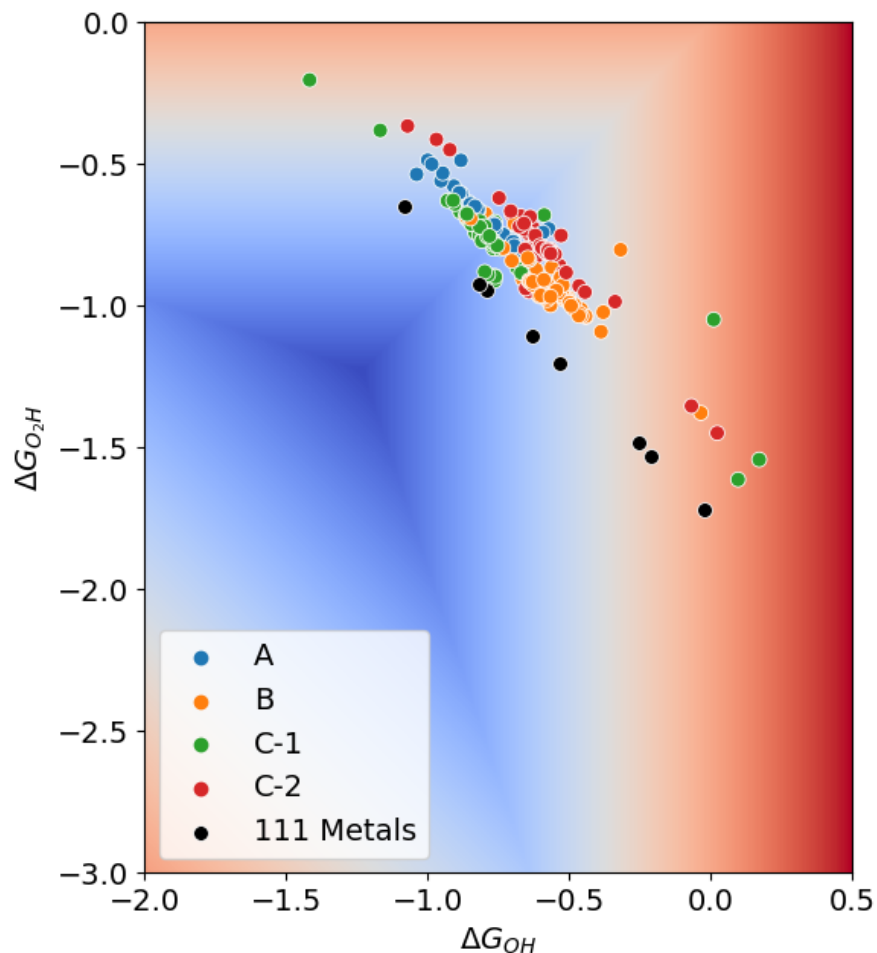


Figure 8: Volcano plot comparing catalysts A, B, and C to previously reported values for 111 metals.⁷

Principal Component Analysis

We applied PCA to visualize the magnitude of the effect of each functional group at the possible locations on the catalysts (**Figure 9**). Each substitution location is depicted with a circle over the hydrogen on the original catalyst; the size of the circle corresponds to how much the intermediate reaction energies changed summed over all substitutions at that location. The circles are split into three colors that each correspond to the first three principal components, where the fraction of the circle is proportional to the magnitude of that principal component's contribution at that site (see **SI** section 2 for a mathematical description).

An immediately striking aspect of these plots is the spatial distribution of the substitution effects. **Figure 9** depicts that while the sites nearer to the active site tend to affect the reaction energies more, the relationship is only approximate. For catalyst A, each substitution site contributes significantly, although the position para to the active site does so more than the meta position. Similarly for catalyst C, the intermediate energies are most sensitive to substitutions that are not

necessarily the nearest site on the catalyst, but instead the atoms that are in strongest resonance with the active site. This is especially apparent for catalyst C, where the two active sites are very sensitive to substitutions at each other's position.

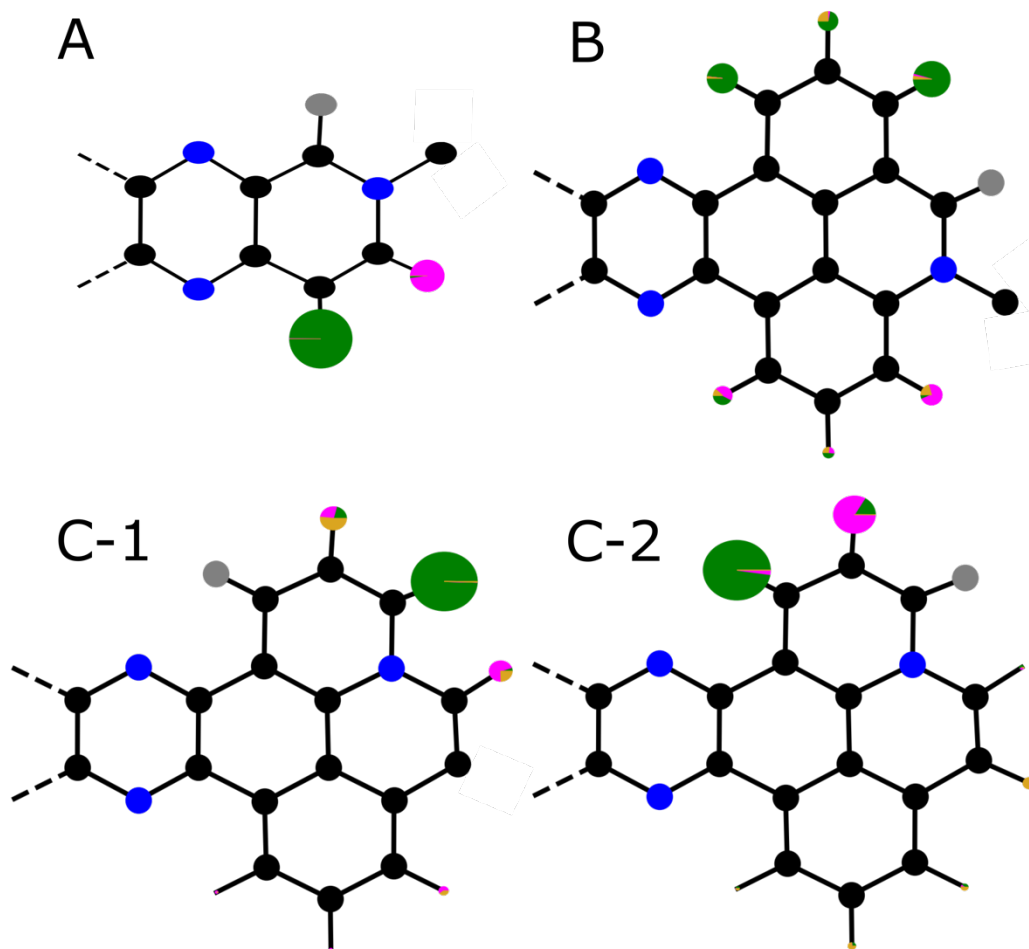


Figure 9: The first three principal components of the effect of functionalizing catalysts A, B, and C mapped onto their molecular structure. The three colors present, (green, pink, and goldenrod) correspond to these three principal components (1st, 2nd, and 3rd, respectively). These components are represented as pie charts, with the size of the pie chart corresponding to the magnitude of the three principal components projected onto that particular functional group site. The fraction of the pie chart for each color corresponds to the contribution for each principal component. The largest pies therefore represent the sites where substitution most strongly affect catalytic activity, and the colors represent the overall effect of general classes of functional groups. The gray circles depict the hydrogen atoms connected to the active sites, which were not substituted. The effect of substitution on one of the hydrogen atoms on catalyst C was not included due to DFT convergence difficulties.

For all catalysts and active sites in **Figure 9**, no more than two principal components are necessary to capture nearly all of the variance. For catalyst A, the first principal component captures how the fluoryl, methoxy, bromyl and methyl functional groups increase the oxygen bonding strength of the catalyst when the modification is para to the active site (**Table S2**), whereas the second component captures how nearly the same set of functional groups—methylamine, methoxy, bromyl, and methyl—deactivate oxygen binding strength when the modification is meta to the active site (**Table S3**). For catalysts B, the effect of the substitutions is almost entirely captured by a single principal component that broadly captures the trend of electron withdrawing groups decreasing the bonding strength of oxygen species and the reverse effect of electron donating groups (**Table S4**). Curiously, the first principal component for C-1 and C-2 captures how various functional groups increase oxygen bonding strength, but the groups—chloryl, methyl, trifluoromethyl, and bromyl for C-1 and methyl, cyanyl, trifluoromethyl, and methylamine for C-2—do not follow the same pattern of electron withdrawing vs donating groups as catalyst B (**Table S5, S6**). A further distinction between C-1 and C-2 is that C-2 exhibits a stronger contribution from the second principal component due to the epoxide structure of the *R* – *O* intermediate at the C-2 active site. PCA thus helps make sense of the complexity of these functional group effects, but additional data is necessary to understand the complexity of the observed deviations on catalyst C from the traditionally expected effects of electron withdrawing and donating groups (**Table S7, S8**).

Applying a linear projection to understand patterns in catalytic activity raises a highly relevant question: how linear are the effects of functional group substitutions? To address this, we generated all possible pairs of functional group substitutions for catalysts B and C, then calculated their O₂ binding energies. For C, we chose to perform calculations only on the C-1 active site. We computed the difference between the O₂ binding energy of the doubly substituted catalysts and the corresponding unsubstituted B or C-1. We also calculated the sum of the binding energy difference for the two singly substituted catalysts with substitutions that correspond to those in the doubly substituted catalysts, and plotted the correlation between the effect of the double substitutions and the sum effect of the individual substitutions on different catalysts (**Figure 10**). The sum effect of the two single substitutions is a good predictor of the effect of double substitutions, especially so for catalyst B and to moderate extent for C-1. The diminished correlation for C-1 may be a result of larger perturbations being less linear in these systems in general, or a sensitivity of catalyst C to multiple substitutions that is not captured by single substitutions. These results indicate that these GCCs may be tuned with multiple functional group substitutions, and that as long as no modifications are made directly to the active site the effects of the substitutions can be predicted relatively reliably using only information about the effects of single substitutions.

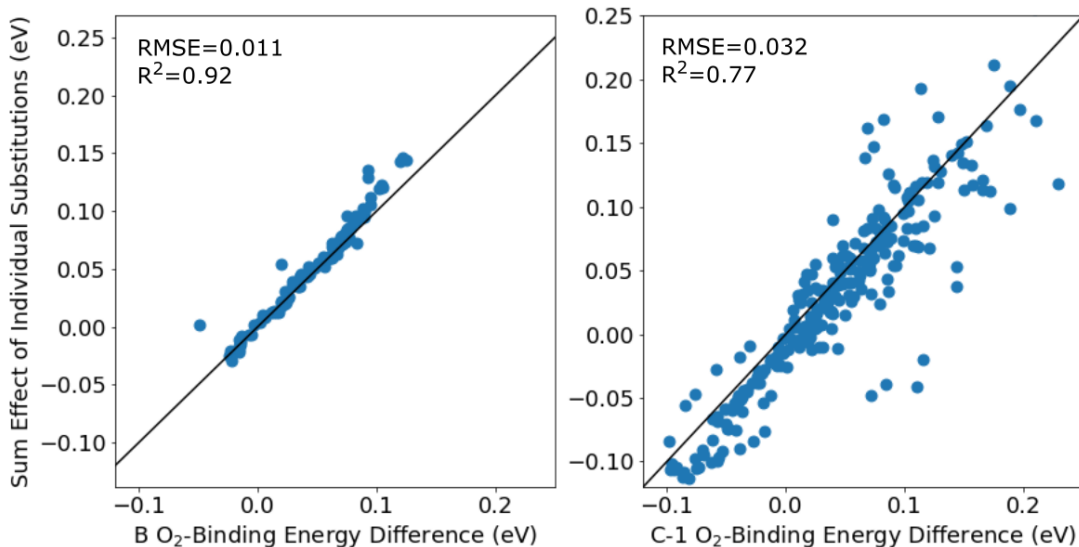


Figure 10: Correlation of two functional group substitutions made to the same catalyst versus the sum of the effects of each substitution on different catalysts.

4. Conclusions

The synthetic flexibility of GCCs offers a wide range of possible heterogeneous catalysts, and we have shown that it is possible to tune intermediate energies and optimize catalysts with simple modifications. We have also provided a framework for understanding the probable locations of active sites. Once a catalytic scaffold is chosen, we have shown that the further effects of simple functional group modifications can be understood and predicted. When the modifications are made to sites that are not the active sites, we have shown that it is possible to understand the effect of these modifications to be altering how readily the catalyst can donate electron density to the bound oxygen species.

We have also shown that structural and functional group modifications have a limited, although not entirely negligible, capacity to break scaling relations between the first and last step of ORR for GCCs. Intriguingly, the epoxide intermediate we observed does create a much stronger deviation from the observed trends for the $R - O_2H + H^+ + e^- \rightleftharpoons R - O + H_2O$ and $R - O + H^+ + e^- \rightleftharpoons R - OH$ steps in the catalytic cycle. Although these steps are not rate limiting for these catalysts, this epoxide intermediate could appear in other nitrogen-doped carbon materials where it could affect catalytic activity. In general, functional group substitutions that caused deviations from the intermediate energy correlations occurred when the modification has a significant effect on the active site. To improve catalytic activity by modifying a known catalyst, one may therefore either take advantage of the predictability of substitutions far from the active site to shift the catalyst along the known scale between strongly and weakly binding active sites, or instead make structural modifications near or directly on the active site to cause more significant changes to activity. This latter method, especially when it changes the way oxygen species bind, seems likely to be the most promising path to breaking scaling relations. This principle is illustrated by the

epoxide intermediate at C-2 that binds more strongly than the singly-bound oxyl species in C-1. This epoxide structure's increased binding strength significantly deviates from the expected strength based on scaling relations relative to other oxygen intermediates. While DFT does not predict this specific deviation will lead to an increased activity for this active site, this does suggest the possibility of engineering future GCCs that can be tuned at multiple active sites, designed to specifically break the other scaling relations that are necessary to improve catalytic activity. Future work could consider catalysts designed using Clar structures to place active sites at the correct spacing to bind both oxygen atoms in O₂ simultaneously. This intermediate could potentially skip the peroxide intermediate entirely and could increase the binding strength of the initial intermediate without increasing the binding strength of the final hydroxide intermediate, definitively deviating from the known scaling relations. Such a catalyst could then be tuned using derivative modifications predicted by DFT to shift intermediate energies without disrupting binding at the active sites.

5. Supporting Information

Section 1 provides additional technical details on how initial geometry preparation for reaction intermediates, as well as the reaction free energy data for the catalytic cycle of all derivatives. Section 2 contains a mathematical description of how PCA was applied to this catalytic cycle data, as well as the principal components. All xyz files for DFT optimized geometries of the catalyst in this study are available at https://figshare.com/articles/dataset/Catalyst_DFT_geometry_xyz_files/22123211.

6. Acknowledgments

This work was supported by a grant from the ACS Petroleum Research Fund (Grant No. 60503-ND6).

7. Notes

The authors have no conflicts of interest to disclose.

8. References

- (1) Stacy, J.; Regmi, Y. N.; Leonard, B.; Fan, M. The Recent Progress and Future of Oxygen Reduction Reaction Catalysis: A Review. *Renew. Sustain. Energy Rev.* **2017**, *69*, 401–414. <https://doi.org/10.1016/j.rser.2016.09.135>.
- (2) Wu, D.; Shen, X.; Pan, Y.; Yao, L.; Peng, Z. Platinum Alloy Catalysts for Oxygen Reduction Reaction: Advances, Challenges and Perspectives. *ChemNanoMat* **2020**, *6* (1), 32–41. <https://doi.org/10.1002/CNMA.201900319>.
- (3) Thorseth, M. A.; Letko, C. S.; Tse, E. C. M.; Rauchfuss, T. B.; Gewirth, A. A. Ligand Effects on the Overpotential for Dioxygen Reduction by Tris(2-Pyridylmethyl)Amine Derivatives. **2012**. <https://doi.org/10.1021/ic301656x>.

- (4) Miner, E. M.; Fukushima, T.; Sheberla, D.; Sun, L.; Surendranath, Y.; Dincø, M. Electrochemical Oxygen Reduction Catalysed by Ni₃(Hexaiminotriphenylene)₂. *Nat. Commun.* **2016**, *7* (10942), 1–7. <https://doi.org/10.1038/ncomms10942>.
- (5) Ward, A. L.; Elbaz, L.; Kerr, J. B.; Arnold, J. Nonprecious Metal Catalysts for Fuel Cell Applications: Electrochemical Dioxygen Activation by a Series of First Row Transition Metal Tris(2-Pyridylmethyl)Amine Complexes. *Inorg. Chem.* **2012**, *51* (8), 4694–4706. <https://doi.org/10.1021/ic2026957>.
- (6) Norskov, J. K.; Ressmeisl, J.; Logadottir, A.; Lindqvist, L.; Kitchin, J. R.; Bligaard, T.; Jonsson, H. Origin of the Overpotential for Oxygen Reduction at a Fuel Cell Cathode. *J. Phys. Chem. B* **2004**, *108*, 17886–17892.
- (7) Kulkarni, A.; Siahrostami, S.; Patel, A.; Nørskov, J. K. Understanding Catalytic Activity Trends in the Oxygen Reduction Reaction. *Chem. Rev.* **2018**, *118* (5), 2302–2312. <https://doi.org/10.1021/acs.chemrev.7b00488>.
- (8) Wroblowa, H. S.; Yen-Chi-Pan; Razumney, G. Electroreduction of Oxygen: A New Mechanistic Criterion. *J. Electroanal. Chem. Interfacial Electrochem.* **1976**, *69* (2), 195–201. [https://doi.org/10.1016/S0022-0728\(76\)80250-1](https://doi.org/10.1016/S0022-0728(76)80250-1).
- (9) Zhang, J. *PEM Fuel Cell Electrocatalysts and Catalyst Layers: Fundamentals and Applications*; Springer Science & Business Media: London, 2008.
- (10) Man, I. C.; Su, H.-Y.; Calle-Vallejo, F.; Hansen, H. A.; Martínez, J. I.; Inoglu, N. G.; Kitchin, J.; Jaramillo, T. F.; Nørskov, J. K.; Rossmeisl, J. Universality in Oxygen Evolution Electrocatalysis on Oxide Surfaces. *ChemCatChem* **2011**, *3* (7), 1159–1165.
- (11) Sheldon, R. A.; Downing, R. S. Heterogeneous Catalytic Transformations for Environmentally Friendly Production. *Appl. Catal. A Gen.* **1999**, *189* (2), 163–183. [https://doi.org/10.1016/S0926-860X\(99\)00274-4](https://doi.org/10.1016/S0926-860X(99)00274-4).
- (12) Fukushima, T.; Drisdell, W.; Yano, J.; Surendranath, Y. Graphite-Conjugated Pyrazines as Molecularly Tunable Heterogeneous Electrocatalysts. *J. Am. Chem. Soc.* **2015**, *137* (34), 10926–10929.
- (13) Virshup, A. M.; Contreras-García, J.; Wipf, P.; Yang, W.; Beratan, D. N. Stochastic Voyages into Uncharted Chemical Space Produce a Representative Library of All Possible Drug-Like Compounds. *J. Am. Chem. Soc.* **2013**, *135* (19), 7296–7303.
- (14) Oh, S.; Gallagher, J. R.; Miller, J. T.; Surendranath, Y. Graphite-Conjugated Rhenium Catalysts for Carbon Dioxide Reduction. *J. Am. Chem. Soc.* **2016**, *138* (6), 1820–1823.
- (15) Kaminsky, C. J.; Wright, J.; Surendranath, Y. Graphite-Conjugation Enhances Porphyrin Electrocatalysis. *ACS Catal.* **2019**, *9* (4), 3667–3671.
- (16) Jackson, M. N.; Surendranath, Y. Molecular Control of Heterogeneous Electrocatalysis through Graphite Conjugation. *Acc. Chem. Res.* **2019**, *52* (12), 3432–3441. <https://doi.org/10.1021/ACS.ACCOUNTS.9B00439>.
- (17) Jackson, M. N.; Kaminsky, C. J.; Oh, S.; Melville, J. F.; Surendranath, Y. Graphite

- Conjugation Eliminates Redox Intermediates in Molecular Electrocatalysis. *J. Am. Chem. Soc.* **2019**, *141* (36), 14160–14167. <https://doi.org/10.1021/JACS.9B04981>.
- (18) Jackson, M. N.; Oh, S.; Kaminsky, C. J.; Chu, S. B.; Zhang, G.; Miller, J. T.; Surendranath, Y. Strong Electronic Coupling of Molecular Sites to Graphitic Electrodes via Pyrazine Conjugation. *J. Am. Chem. Soc.* **2018**, *140* (3), 1004–1010.
- (19) Oh, S.; Bisbey, R. P.; Gul, S.; Yano, J.; Fisher, G. L.; Surendranath, Y. N-Heterocyclic Linkages Are Produced from Condensation of Amidines onto Graphitic Carbon. *Chem. Mater.* **2020**, *32* (19), 8512–8521. <https://doi.org/10.1021/ACS.CHEMMATER.0C02664>.
- (20) Jackson, M. N.; Pegis, M. L.; Surendranath, Y. Graphite-Conjugated Acids Reveal a Molecular Framework for Proton-Coupled Electron Transfer at Electrode Surfaces. *ACS Cent. Sci.* **2019**, acscentsci.9b00114.
- (21) Hohenberg, P. Inhomogeneous Electron Gas. *Phys. Rev.* **1964**, *136* (3B), B864–B871. <https://doi.org/https://doi.org/10.1103/PhysRev.136.B864>.
- (22) Kohn, W.; Sham, L. J. Self-Consistent Equations Including Exchange and Correlation Effects. *Phys. Rev.* **1965**, *140* (4A), A1133–A1138.
- (23) Lodaya, K.; Ricke, N. D.; Chen, K.; Van Voorhis, T. Machine Learning Identification of Active Sites in Graphite-Conjugated Catalysts. *J. Phys. Chem. C* **2023**, *127*, 2303–2313. <https://doi.org/10.1021/ACS.JPCC.2C07876>.
- (24) Clar, E. *The Aromatic Sextet*; Wiley Interscience: London, 1972.
- (25) Shao, Y.; Gan, Z.; Epifanovsky, E.; Gilbert, A. T. B.; Wormit, M.; Kussmann, J.; Lange, A. W.; Behn, A.; Deng, J.; Feng, X.; et al. Advances in Molecular Quantum Chemistry Contained in the Q-Chem 4 Program Package. *Mol. Phys.* **2014**, *113* (2), 184–215. <https://doi.org/10.1080/00268976.2014.952696>.
- (26) Tao, J.; Perdew, J. P.; Staroverov, V. N.; Scuseria, G. E. Climbing the Density Functional Ladder: Nonempirical Meta-Generalized Gradient Approximation Designed for Molecules and Solids. *Phys. Rev. Lett.* **2003**, *91* (14), 146401.
- (27) Hehre, W. J.; Ditchfield, R.; Pople, J. A. Self-Consistent Molecular Orbital Methods. XII. Further Extensions of Gaussian-Type Basis Sets for Use in Molecular Orbital Studies of Organic Molecules. *J. Chem. Phys.* **1972**, *56* (5), 2257–2261.
- (28) Ditchfield, R.; Hehre, W. J.; Pople, J. A. Self-Consistent Molecular-Orbital Methods. IX. An Extended Gaussian-Type Basis for Molecular-Orbital Studies of Organic Molecules. *J. Chem. Phys.* **1971**, *54* (2), 724–728.
- (29) Clark, T.; Chandrasekhar, J.; Spitznagel, G. W.; Schleyer, P. V. R. Efficient Diffuse Function-Augmented Basis Sets for Anion Calculations. III. The 3-21+G Basis Set for First-Row Elements, Li-F. *J. Comput. Chem.* **1983**, *4* (3), 294–301.
- (30) Cancès, E.; Mennucci, B.; Tomasi, J. A New Integral Equation Formalism for the Polarizable Continuum Model: Theoretical Background and Applications to Isotropic and Anisotropic Dielectrics. *J. Chem. Phys.* **1997**, *107* (8), 3032.

- (31) Halgren, T. A. Merck Molecular Force Field. I. Basis, Form, Scope, Parameterization, and Performance of MMFF94. *J. Comput. Chem.* **1996**, *17* (5–6), 490–519. [https://doi.org/10.1002/\(SICI\)1096-987X\(199604\)17:5/6<490::AID-JCC1>3.0.CO;2-P](https://doi.org/10.1002/(SICI)1096-987X(199604)17:5/6<490::AID-JCC1>3.0.CO;2-P).
- (32) Momma, K.; Izumi, F. VESTA: A Three-Dimensional Visualization System for Electronic and Structural Analysis. *J. Appl. Crystallogr.* **2008**, *41* (3), 653–658.
- (33) Mavros, M. G.; Tsuchimochi, T.; Kowalczyk, T.; Mclsaac, A.; Wang, L.-P.; Voorhis, T. Van. What Can Density Functional Theory Tell Us about Artificial Catalytic Water Splitting? *Inorg. Chem.* **2014**, *53* (13), 6386–6397.
- (34) Landrum, G. RDKit: A Software Suite for Cheminformatics, Computational Chemistry, and Predictive Modeling. **2013**.
- (35) Ricke, N. D.; Murray, A. T.; Shepherd, J. J.; Welborn, M. G.; Fukushima, T.; Van Voorhis, T.; Surendranath, Y. Molecular-Level Insights into Oxygen Reduction Catalysis by Graphite-Conjugated Active Sites. *ACS Catal.* **2017**, *7* (11), 7680–7687. <https://doi.org/10.1021/acscatal.7b03086>.
- (36) Lodaya, K.; Ricke, N. R.; Chen, K.; Van Voorhis, T. Machine Learning Identification of Active Sites in Graphite-Conjugated Catalysts. *ChemRxiv* **2022**.
- (37) Behn, A.; Zimmerman, P. M.; Bell, A. T.; Head-Gordon, M. Efficient Exploration of Reaction Paths via a Freezing String Method. *J. Chem. Phys.* **2011**, *135* (22), 224108. <https://doi.org/10.1063/1.3664901>.
- (38) Sharada, S. M.; Zimmerman, P. M.; Bell, A. T.; Head-Gordon, M. Automated Transition State Searches without Evaluating the Hessian. *J. Chem. Theory Comput.* **2012**, *8* (12), 5166–5174. <https://doi.org/10.1021/CT300659D>.
- (39) Solà, M. Forty Years of Clar's Aromatic π -Sextet Rule. *Front. Chem.* **2013**, *0*, 22. <https://doi.org/10.3389/FCHEM.2013.00022>.

Clar structures
identify active sites

